Influence of Ti and Co/Ni Ratio on the Oxidation at 1200 °C of Chromium-Containing Ni, Co-Based Cast Alloys

Patrice Berthod, Synthia Annick Ozouaki Wora

Preprint version of:

“Influence of Ti and Co/Ni Ratio on the Oxidation at 1200 °C of Chromium-Containing {Ni, Co}–Based Cast Alloys”

Patrice Berthod, Synthia Annick Ozouaki Wora

Metallurgical and Materials Transactions A: Physical Metallurgy and Materials Science, 2022, 53A, 277–289.

Behavior in oxidation at elevated temperature of titanium–containing {Ni, Co}–based cast alloys rich in chromium

Patrice Berthod[1,2,*], Synthia Annick Ozouaki Wora[2]

[1]*Université de Lorraine, CNRS, IJL, Nancy, France*
[2]*Université de Lorraine, FST, Vandoeuvre-lès-Nancy, France*
**Corresponding author : patrice.berthod@univ-lorraine.fr*

Abstract. This work consists in an investigation of the possible influence that titanium may be have on the oxidation of {nickel and/or cobalt}–based chromium–rich alloys, and in the affirmative way the aspects of this behavior may be affected. It starts with the elaboration by casting of a series of alloys from pure elements, with a base element ranging from nickel only to cobalt only. To magnify these possible effects of titanium, more than 1 wt.% Ti was introduced in the chemical composition, more precisely 1.6 wt.% in order to reach the atomic equivalence with the carbon present (0.4wt.% C). To amplify the oxidation process, the oxidation tests carried out in laboratory air were run at the constant temperature of 1200°C during a rather long time (170h). The surface states and cross–sections were characterized by XRD, electron microscopy and EDS analyses. The results demonstrates that all the alloy (except the nickel–free cobalt–based one) resisted oxidation rather well without catastrophic evolution due to titanium. The tested Ti content led to significant internal oxidation and to an external selective oxidation producing a thin layer stick on the outer side of the chromia scale. It is supposed that this outermost TiO2 layer may be beneficial for the oxidation behavior by the possible limitation of the deleterious over–consumption of chromium by chromia re–oxidation/volatilization.

Keywords: Cast alloys; Nickel and cobalt; Titanium; High temperature oxidation; Metallography characterization

INTRODUCTION

In order to achieve high level of mechanical properties at high temperature, particular elements are generally added to alloys and superalloys to reinforce them by solid solution strengthening or by precipitation strengthening [1, 2]. During service at high temperature in oxidant atmospheres, these same added elements can be involved in oxidation phenomena These elements may play a role in the global behavior of the alloys, notably since they are often more oxidable than the base elements [3, 4]. Among them, titanium – which can be found in the gamma prime precipitates of some nickel–based single crystalline superalloys [5,6] – spontaneously forms oxides and nitrides at high temperature. This element can be also present in superalloys based on nickel and cobalt simultaneously [7], recent cobalt alloys [8] even single crystalline [9]. Beside intermetallic compounds titanium is also often encountered in superalloys as TiC carbides. Conventionally cast nickel–based alloys are particularly concerned [10,11], but also nickel–based single crystals [12, 13], coatings and composites [14, 15].

Titanium monocarbides are of the same carbides family as other MC, e.g. TaC or HfC. Furthermore, when they form in significant quantity in superalloys solidifying in conventional conditions (i.e. not directionally or as single – crystals) they may appearing at the end of solidification as eutectic carbides with Chinese script shape. This particular morphology, observed for instance in polycrystalline equi–axed chromium–rich cobalt–based superalloys [16, 17], was identified as potentially very beneficial for the strength at elevated temperature. Indeed TaC also presents this morphology in creep–resistant Co(Ni)–based industrial superalloys [18] and in Fe–based alloys [19], and HfC too in Co–based [20] and Ni–based [21] academic alloys. The carbides of titanium has the advantage of a lower density by comparison with the ones of the other monocarbides which involve much heavier metallic elements such as Ta or Hf, with as consequence slight lowering of the volume mass of the whole alloy.

But titanium is also extremely oxidable and its easy and fast reaction with oxygen – after outwards diffusion of Ti as well as after inwards diffusion of oxygen – may influence the progress of oxidation. Different scenarios may be expected from its particular behavior for chromia–forming alloys: can it lead to the formation of single or mixed oxides in the external oxide scale (possibly disturbing chromia growth)? Can it take part to the constitution of an interfacial oxide separating alloy and the chromia scale with good or bad influence of the adherence of the later (as $CrTaO_4$ forming for tantalum–containing alloys [22])? Is internal oxidation the single oxidation mode for titanium as for hafnium in HfC–reinforced chromia–forming alloys [23]? Other questions which can be also asked are: if the

carbides network is composed of a great part of TiC, have these ones a tendency to disappear from the oxidation front to develop a carbide–free zone as TaC [22]? Or not as HfC [23]? For the oxidation process as for the loss of carbides in the subsurface, the conditions of titanium diffusion in situation of oxidation are also of importance, and this may depend on the matrix nature. To try answering these questions, a series of alloys, based on different Co and Ni mixtures all containing 25wt.%Cr, 0.4C and 1.6Ti (for the atomic equivalence between Ti and C), all contents being in weight percent, were elaborated and their microstructures and high temperature oxidation behaviors were investigated.

EXPERIMENTAL

The chemical compositions of the alloys elaborated for this study are presented in Table 1. There are three Ni–richest alloys (from the cobalt–free "0Co5NiTi" alloy to the "2Co3NiTi" alloy) and three Co–richest alloys (from the "3Co2NiTi" alloy to the nickel–free "5Co0NiTi" alloy). The preparations were composed of pure elements (Alfa Aesar, more than 99.9wt.% for their purity). Each of them was cast using high frequency induction melting in inert atmosphere (CELES furnace operating at up to 5,000 Volts at 100,000–110,000 Hertz, fusion chamber closed by a water–cooled copper crucible and a silica tube, 0.3 bar of pure Ar)). Melting was achieved two times successively to be sure to be free of not–molten parts.

The obtained ingots, each with a 40 grams mass and an ovoid shape, were cut using a metallography saw to obtain parts for the examination of the as–cast microstructures and parts for the exposures to laboratory air at high temperature. The parts for preliminary metallography were embedded in a mixture of Araldite resin and hardener (ESCIL) and, after total rigidification and extraction out of the plastic molds, ground/polished with SiC papers and micrometric alumina–enriched textile disks in order to obtain mirror–like samples for observations.

The rest of the ingot was cut in two halves which were ground until the 1200–grade of SiC paper on the two main faces, with smoothing of the edges to avoid local overoxidation. These samples were each placed in an alumina shuttle and six shuttles each containing one of the six alloys were put in the hot zone of a muffle resistive furnace. Here they were heated together up to 1200°C. After 170 hours of exposure to laboratory air at this temperature, the furnace was shut off and the oxidized samples cooled in the furnace still closed.

The oxides spalled off during cooling and remaining in the ceramic shuttles were collected and analyzed by X–ray diffraction (XRD), while the ones remaining on the surfaces of the oxidized samples were observed and analyzed by Energy Dispersion Spectrometry (EDS) on cross-section preparations obtained by embedding in cold resin mixture, cutting, grinding and polishing. The as–cast and aged bulk microstructures of the alloys before and after oxidation test, as well as the oxides still stuck on surface and the oxidation–induced microstructure changes in subsurface, were observed using a Scanning Electron Microscope JSM 6010 LA from JEOL. Spot analyses were carried out with the EDS device equipping the SEM to identify external and internal oxides, the chemical composition in the outermost part of the alloys and to obtain concentration profiles for chromium and titanium from the oxidation front towards the bulk.

RESULTS

Microstructures of the obtained alloys

The microstructures of the six alloys after their syntheses by casting are illustrated by SEM micrographs taken in Back Scattered Electrons mode (BSE). These micrographs are presented in Figure 1. There are three common points between these alloys: a polycrystalline equi–axed matrix, interdendritic carbides forming a eutectic with matrix, and a microstructure fineness characterized by about 25 µm for the secondary dendrite arm spacing. In contrast, the nature of the carbides varies from the cobalt–free nickel–based 0Co5NiTi alloy (only acicular chromium carbides) and the nickel–free cobalt–based 5Co0NiTi alloy (only script–like titanium carbides).

Oxidized states examination and characterization prior to cutting

A quarter of each ingot was exposed to laboratory air for 170 hours at 1250°C. After cooling to room temperature these samples were more or less covered by external oxide scales and surrounded by oxides detached from their surfaces. The states of the oxidized surfaces of the two flat faces are shown by macrophotographs in Figure 2. The oxides collected all around each sample (in the alumina shuttles) were subjected to X–ray diffraction (two of the obtained XRD diffractograms in Figure 3 and Figure 4).

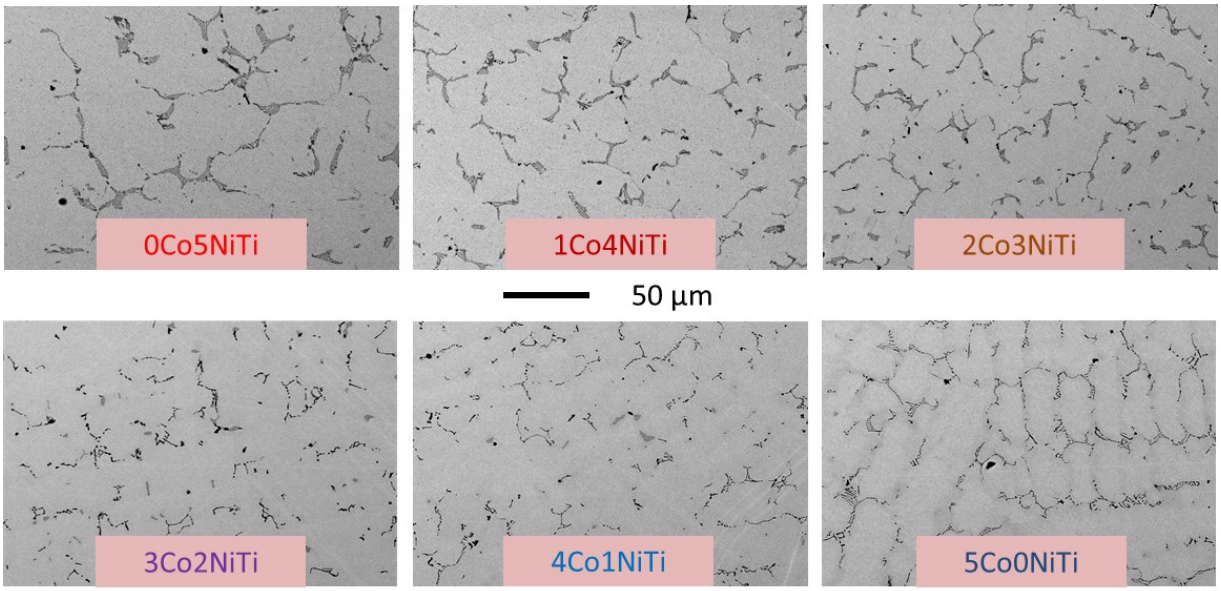

FIGURE 1. The as–cast microstructures of the six alloys of the study (SEM/BSE, ×500)

Obviously, spallation did not take place similarly between the nickel–richest alloys (two top lines of Figure 2) and the cobalt–richest ones (two bottom lines of Figure 2). The 0Co5NiTi, 1Co4NiTi and 2Co3NiTi alloys were here and there totally denuded because of the local loss of all the thickness of external oxide (bright areas). The 3Co2NiTi, 4Co1NiTi and 5Co0NiTi alloys are still wholly covered by dark gray oxide but the external aspect of the scales is not homogenous (smooth or rough), and the thickness seems also different between areas on a same sample. These last samples were too surrounded by oxides having obviously lost their surfaces.

The oxides lost by each sample were collected separately and XRD runs were carried out to determine their nature. Two examples of obtained diffractograms are given in Figure 3 (oxides collected around one of the Ni–richest alloys) and in Figure 4 (oxides collected around one of the Co–richest alloys), and the whole obtained results are presented together in Table 2. XRD allowed evidencing that two oxides formed on all the samples: chromia (Cr_2O_3) and titanium dioxide (TiO_2). Spinel oxides also formed as soon as the cobalt content became equal to – or higher than – 15wt.%. $NiCr_2O_4$ or $(Ni,Cr)_2O_4$ for the cobalt–containing Ni–richest alloys, and $CoCr_2O_4$ for the Co–richest alloys.

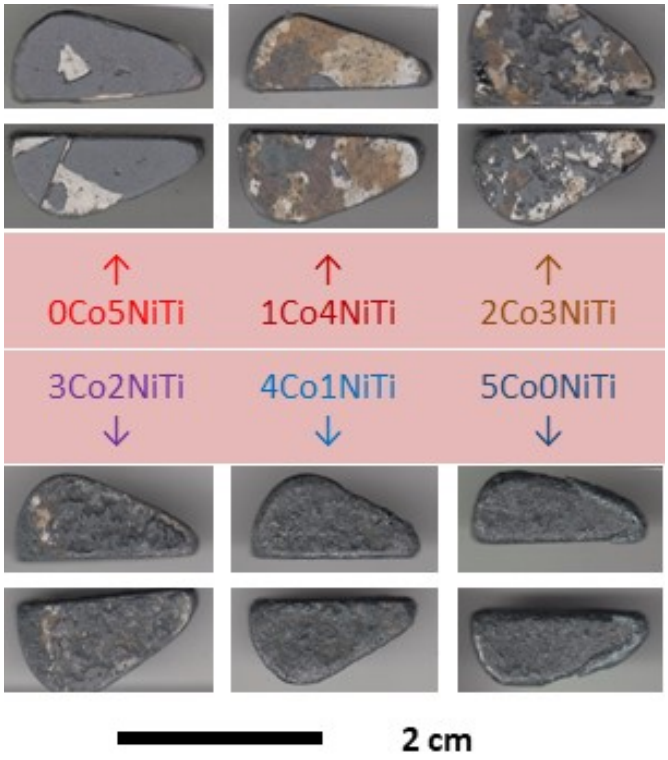

FIGURE 2. Photographs of the two main faces of the six samples after oxidation

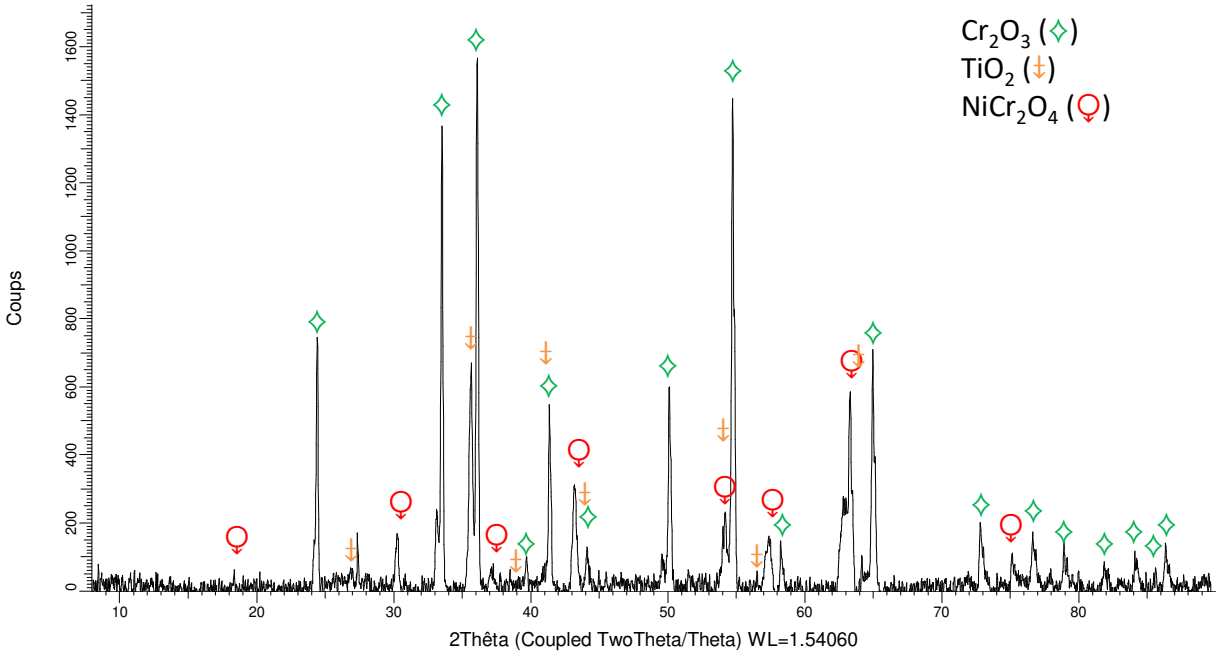

FIGURE 3. Example of XRD pattern: here the oxidized surface of the 1Co4NiTi alloy

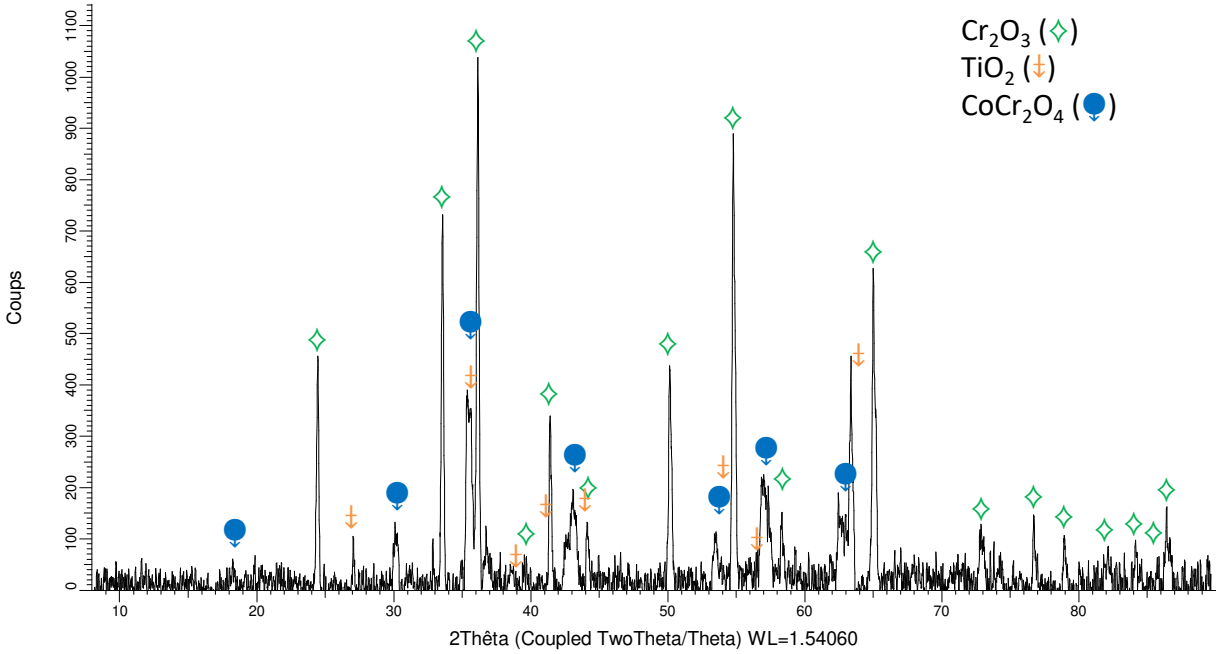

FIGURE 4. Example of XRD pattern: here the oxidized surface of the 4Co1NiTi alloy

Cross–sectional examination and qualitative characterization of the oxidized states

After embedding, transversal cutting, grinding and polishing the oxidized surfaces and subsurfaces were observed in cross–section (Figure 5 and Figure 6). The different types of oxides still stuck on surface and the internal oxides were identified by EDS spot analysis (Figure 6, Table 3).

Seen in cross–section, it appears that the external oxide scale is mainly composed of chromia which obviously developed as a thick layer in contact with the metallic substrate. A continuous layer of titanium oxide has formed too, above chromia (i.e. separating it from air during the high temperature exposure). During cooling, the outermost oxide TiO_2 has been lost here and there without or with the corresponding part of chromia. In the case of the alloys which are the richest in cobalt, shear rupture obviously occurred and the inner part of the chromia scale remained stuck on the alloy while the outer chromia and the outermost TiO_2 scale quitted the samples. For these later Co–rich alloys, one also notices a start of inward progress of oxidation, revealed by an irregular oxide/alloy frontier and, in some location, a deep penetration of oxidation. For the same Co–richest alloys, the presence of thick $CoCr_2O_4$ mixed with CoO oxides suggests that generalized oxidation was taking place in these locations.

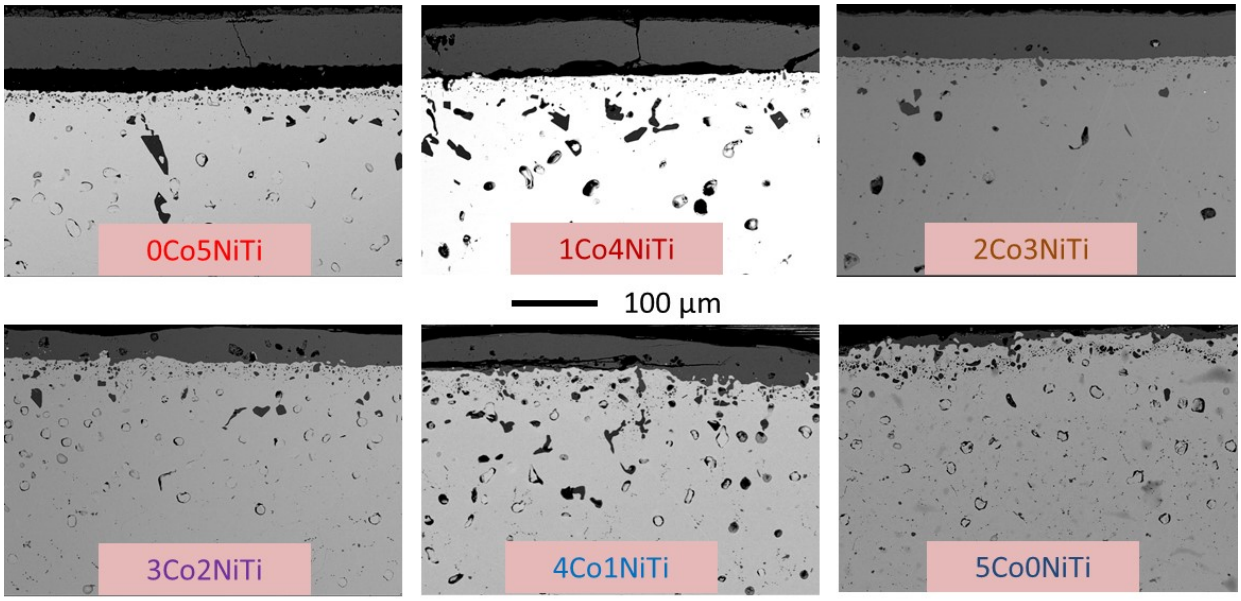

FIGURE 5. Electronic micrographs illustrating the surface states of the oxidized alloys (SEM/BSE, ×250)

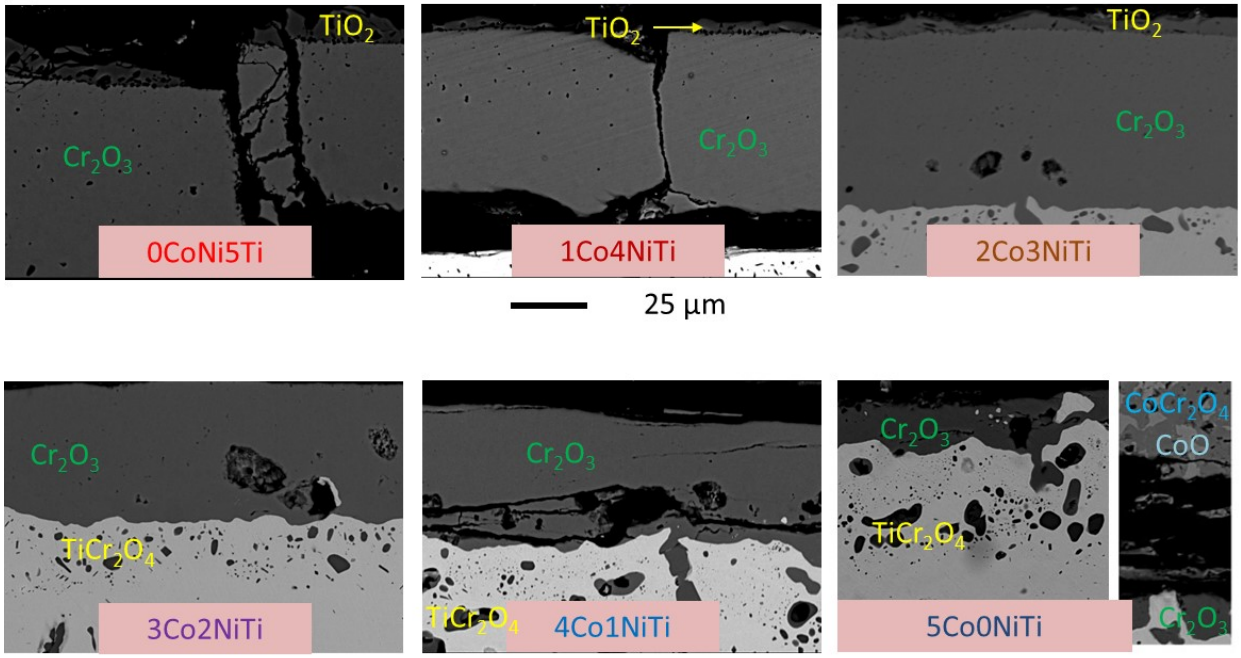

FIGURE 6. Electronic micrographs illustrating the surface states of the oxidized alloys (SEM/BSE, ×1000)

In the subsurface, on can observe a more or less deep extension of a phenomenon of disappearance of carbides (chromium carbides and/or titanium carbides) as well as internal oxidation (internal chromia, but the most often $TiCr_2O_4$). There are also many porosities that formed, seemingly. The list of the oxides observed in cross–section in the external oxide scales and in the subsurface are recapitulated in Table 3. By comparison with Table 2 one can see that the most part of the spinel oxides were lost with the oxide scales spalled off during cooling while $TiCr_2O_4$ were logically kept in the alloys since they essentially formed internally.

Quantitative characterization of the oxidized states

Several parameters characterizing the oxidation products or the degradation caused by oxidation to the alloys were subjected to measurements. The thickness of the chromia scale is plotted in Figure 7 together with the one of the outermost TiO_2 scale (five values per alloy). The chromia scale was particularly preserved from spallation for the cobalt–free alloy (0Co5NiTi); the thickness is the greatest and the scale is regular. The average value decreases when Co is present in the alloy while the standard deviation increases significantly. This reveals a loss of a part of thickness by shear rupture during cooling: this moss seems limited for the alloys with rather equilibrated contents in Co and Ni, but greater for the two Co – richest alloys (4Co1NiTi and 5Co0NiTi). The TiO_2 thickness follows the same trend. As soon as the outer part of chromia was lost the corresponding outermost TiO_2 was lost too. The average TiO_2 thickness is maximal for the 0Co5NiTi alloy, lower for the 1CoNiTi and 2Co3NiTi alloys, and lost everywhere for the cobalt–richest alloys.

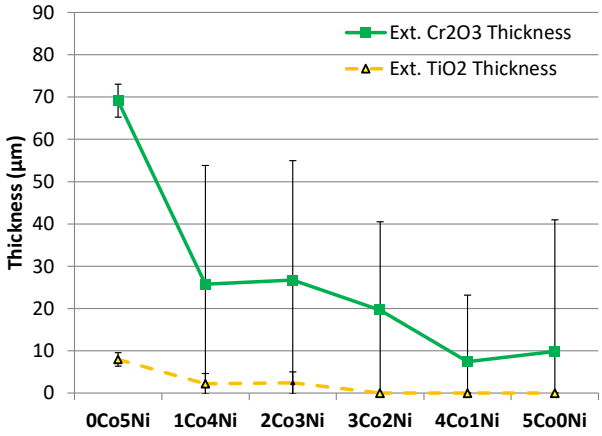

FIGURE 7. Thicknesses of the two main oxides of the continuous external scale: Cr_2O_3 and TiO_2 (outermost oxide)

After the external oxides, the distribution of the two principal types of internal oxides was also characterized, by measuring the depth of existence of these internal oxides from the scale/alloy interface (five values per alloy). Results are plotted together in Figure 8. The depth of appearance of the oxides involving chromia (internal Cr_2O_3 and $TiCr_2O_4$) is obviously maximal for the two Ni–richest alloys (≈ 30–70 µm) and lower for the four other alloys (≈ 20–25 µm). Seemingly TiO_2 formed significantly deeper, from (≈ 125 µm) for the two Ni–richest alloys and lower for the four other alloys (≈ 80 µm).

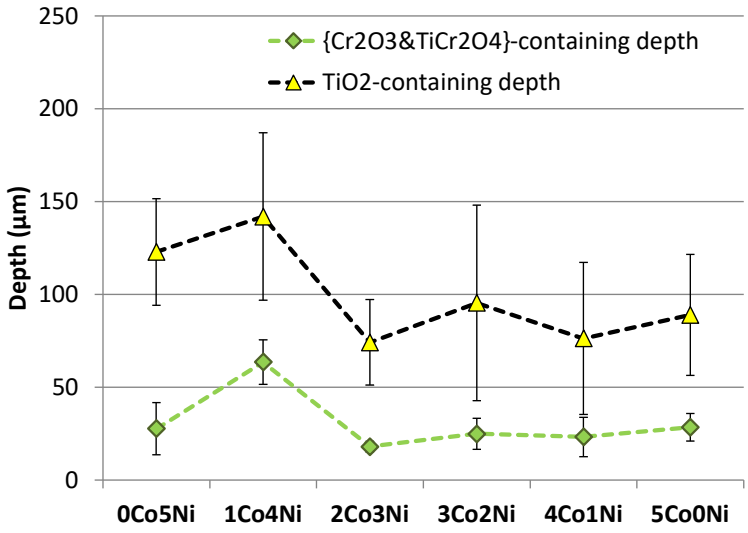

FIGURE 8. Depth of presence of internal Cr_2O_3 / $TiCr_2O_4$ and TiO_2 in the subsurface

Another consequence of oxidation for the subsurface is the disappearance of carbides. The depth of carbide disappearance, again counted from the oxide scale/alloy interface, was measured (five values per alloy) for the two types of carbides, chromium carbides and titanium carbides. The depth of carbide disappearance decreases with the increase in cobalt in the alloy. The chromium carbides are more affected by the disappearance phenomenon that the titanium carbides: globally the depth of chromium carbide disappearance is twice the one of the TiC carbides. For the 0Co5NiTi alloy which contains only chromium carbides there is no depth of TiC disappearance. Similarly, for the two Co – richest alloys which did not contain chromium carbides, only the TiC disappearance depth had some signification.

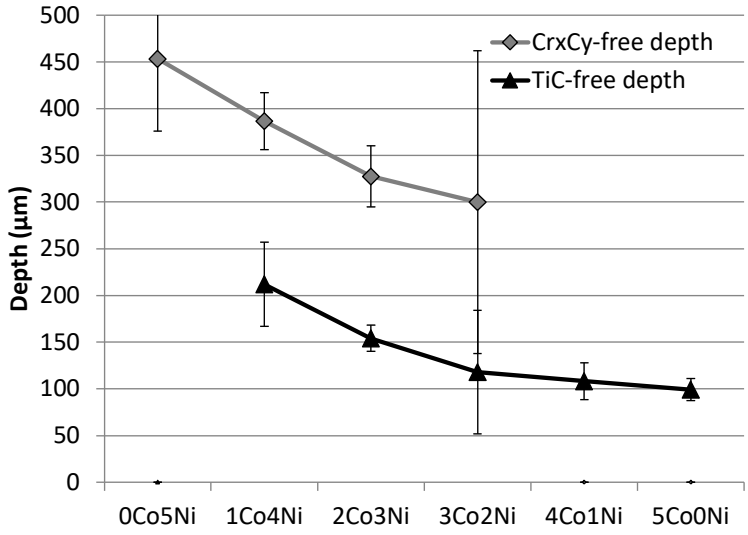

FIGURE 9. Depths of disappearance of chromium carbides and titanium carbides

A series of chemical measurements were carried out in extreme surface and deeper in the subsurface. EDS spot analysis was performed in the alloy very close to the {oxide scale / alloy} interface. The obtained contents in chromium and tantalum are graphically presented in Figure 10. Due to oxidation the local chromium content has decreased down to values equal to 16 wt.% Cr for the Ni–richest alloy and even lower for the other alloys. Indeed the Cr content in the outermost part of alloy decreases progressively with the presence of more and more cobalt, from the 16 wt.% for the 0Co5NiTi alloy to slightly lower than 15 wt.% for the 5Co0NiTi alloy. In the same time the titanium content varies too but with no systematic trend.

Concentration profiles were acquired inwards from the {oxide scale / alloy} interface. They are shown in Figure 11 for chromium and in Figure 12 for titanium. One finds again the slight decrease in chromium content in extreme surface when the alloy contains more and more cobalt. These profiles additionally show that the chromium–depleted zone is not really different between the six alloys (about 300 µm for all of them), but the maximal concentration gradients in chromium (linear parts over the first 200 µm from the {oxide scale / alloy} interface) are seemingly higher for the Co–richest alloys than for the Ni–richest ones. The titanium concentration profiles are much more irregular, perturbed by the presence of a dense population of titanium oxides. This does not allows comparing them to one another efficiently. There is seemingly no correspondence between the depths of the carbide–free zones neither with the chromium–depleted depths, nor with the high Cr gradient parts in the concentration profiles.

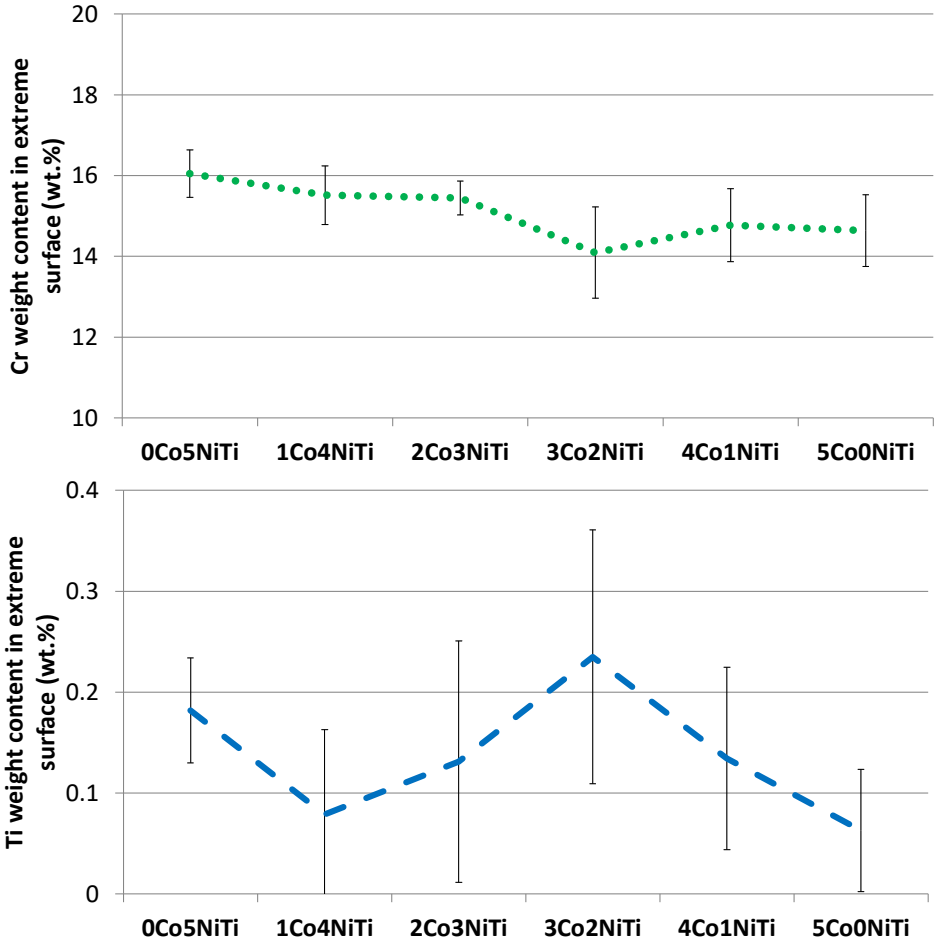

FIGURE 10. Chromium (top) and titanium (bottom) contents in the outermost part of the alloys

Evolution of the microstructure in the bulk

Microstructure observation with the SEM was carried out deeper, in the center of the samples. The initial microstructures of the three Ni–richest alloys are reminded, with a higher magnification than in Figure 1, in the top part of Figure 13 and in the top part of Figure 14 for the three Co–richest alloys. In the bottom parts of these figures the corresponding SEM micrographs taken in the bulk of the alloys after exposure at 1200°C for 170 hours, evidence the morphological evolution of the carbides. The chromium carbides (medium gray), which were finely structured (acicular–shaped) have considerably coarsened. The titanium carbides have themselves significantly changed; they become very round too.

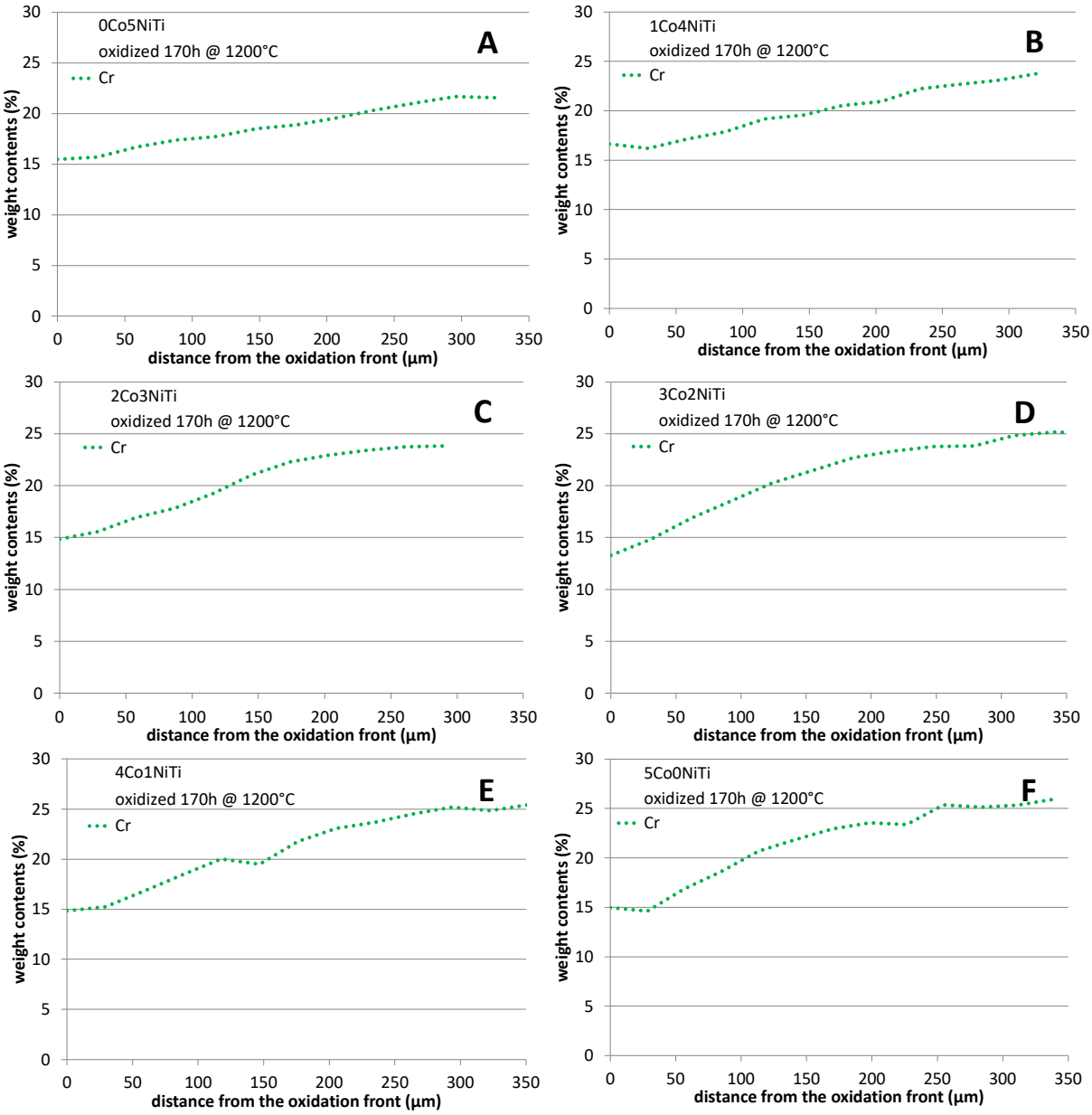

FIGURE 11. Concentrations profiles in chromium from the oxide scale / alloy interface (SEM/EDS);

A: 0Co5NiTi, B: 1Co4NiTi, C: 2Co3NiTi, D: 3Co2NiTi, E: 4Co1NiTi, F: 5Co0NiTi

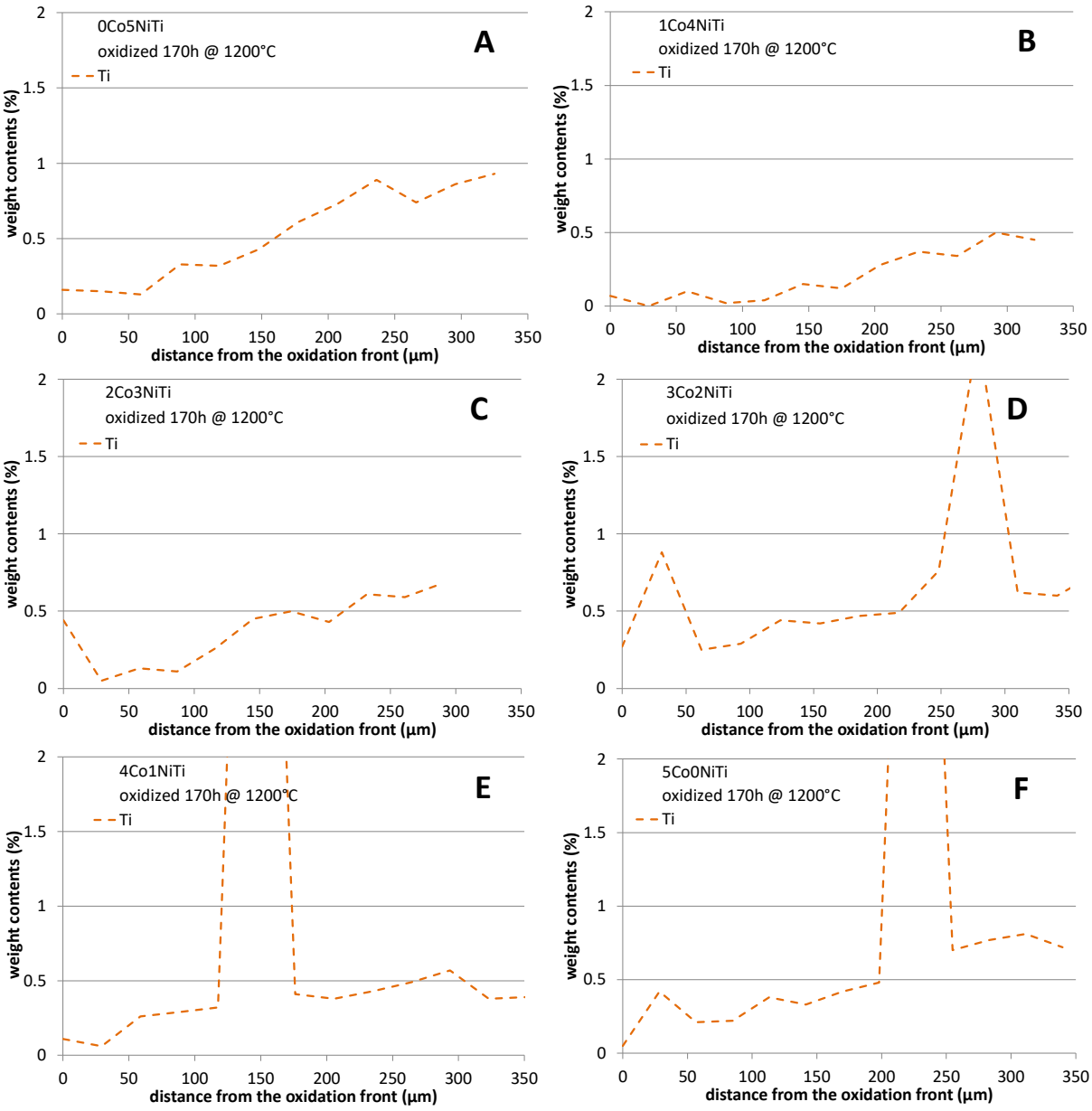

FIGURE 12. Concentrations profiles in titanium from the oxide scale / alloy interface (SEM/EDS);

A: 0Co5NiTi, B: 1Co4NiTi, C: 2Co3NiTi, D: 3Co2NiTi, E: 4Co1NiTi, F: 5Co0NiTi

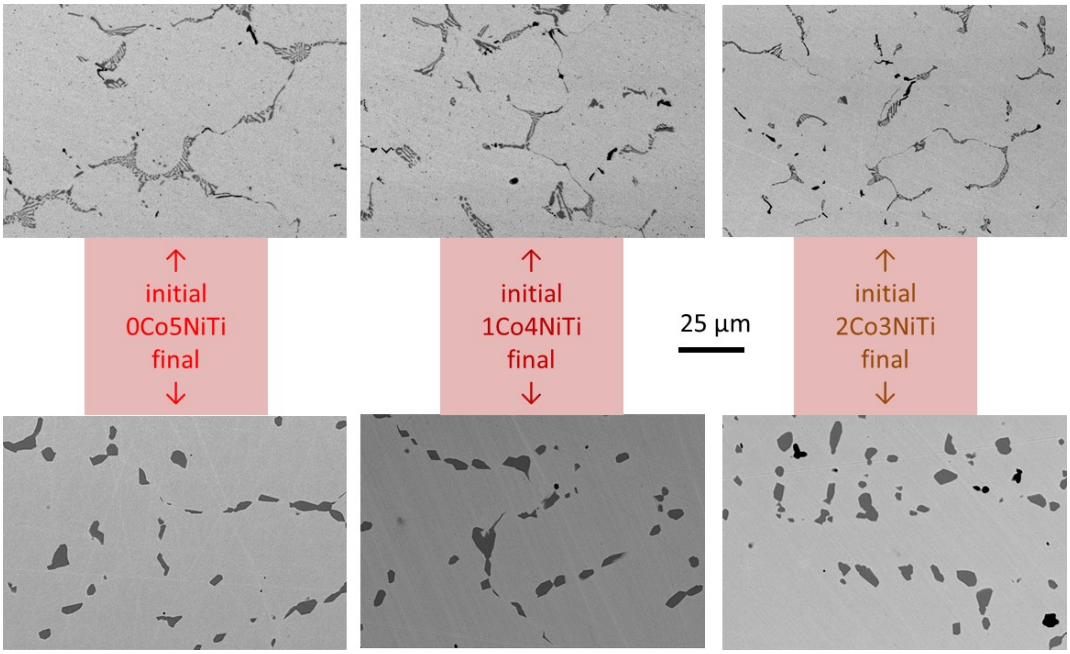

FIGURE 13. Electronic micrographs illustrating the initial and final microstructures in the bulk of the three Ni–richest alloys (SEM/BSE, ×1000)

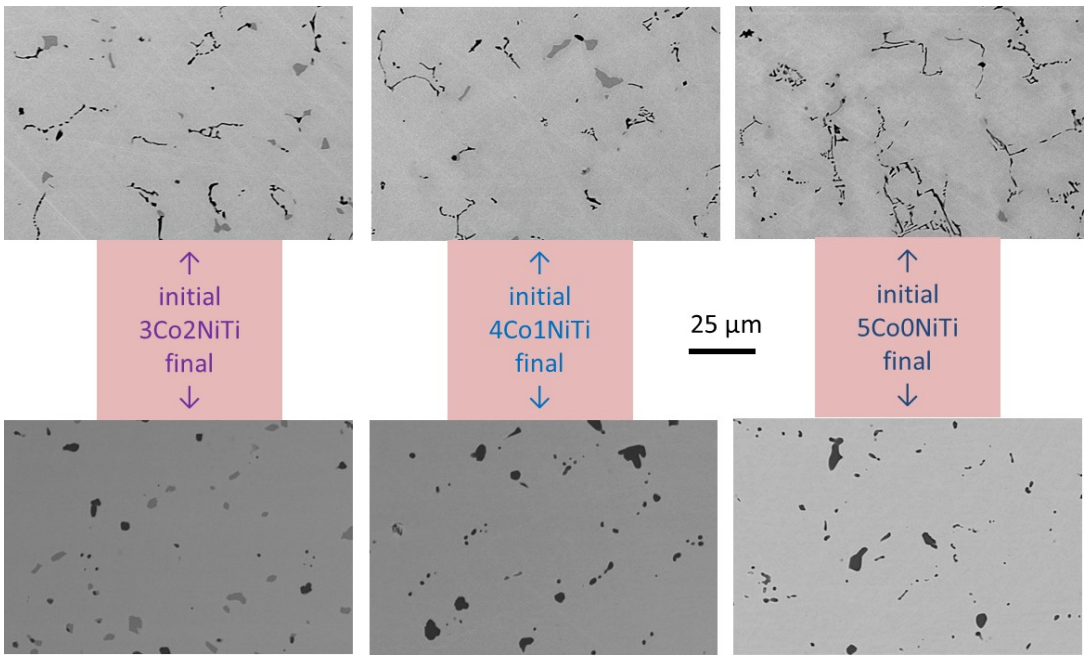

FIGURE 14. Electronic micrographs illustrating the initial and final microstructures in the bulk of the three Co–richest alloys (SEM/BSE, ×1000)

DISCUSSION

Obviously, the addition of titanium to {Ni, Co}–25wt.%Cr–0.4wt.%C alloys did not lead systematically to titanium carbides. However titanium is known as a strong carbide–former metal and TiC are among the most stable carbides [24, 25]. In most of the alloys of the present work titanium undergoes competition from chromium. In their as–cast states, this led to the simultaneous presence of chromium carbides and titanium carbides in the three medium alloys containing 29 wt.% Co and more (from 2Co3NiTi to 4Co1NiTi). For 15 wt.%Co and less (1Co4NiTi and 0Co5NiTi) chromium carbides are nearly the single carbide phase present. TiC carbides are alone only in the nickel–free Co–based alloy 5Co0NiTi. The carbides had morphologically evolved but their natures and proportions were the same at the end of the long exposures at elevated temperatures resulting from the oxidation tests, principal object of this study. This showed that the double population of chromium carbides and titanium carbides did not result from non–equilibrium crystallization (because fast solidification in the copper crucible of the high frequency induction furnace) but corresponds to the metallurgical state stable at this temperature.

Concerning their behaviors in oxidation, one can say that the alloys rather well resisted, taking into account the long time of exposure to air and the high level of temperature. The main chemical parameter governing the level of hot oxidation resistance was not really titanium but the nickel and cobalt relative proportions in the alloys: external chromia for the nickel–rich alloys, and chromia added with significant quantities of $CoCr_2O_4$ spinel, and even CoO for the alloys richest in cobalt, notably free of nickel (5Co0NiTi alloy). NiO and $NiCr_2O_4$ were also detected for the Ni – rich alloys, but in much lower quantities. Much cobalt or cobalt – chromium oxides for the cobalt–richest alloys (suggesting the start of generalized oxidation, inwards progressing) and only few nickel and nickel–chromium oxides for the nickel–richest alloys, was the main difference of oxidation behavior between these two types of alloys.

Furthermore, it was easily observed that the alloys richest in nickel developed only a double external oxide scale, composed of a thick continuous chromia scale in contact with the alloy substrate, topped with a thin continuous TiO_2 layer isolating chromia from hot air. This was clearly seen where this external oxides sandwich remained on the alloy despite the tendency to spallation during cooling. Whatever it happened during cooling, collecting the lost oxides and analyzing them with the X–ray diffractometer allowed seeing that TiO_2 was present in the external scale even for the alloys richer in cobalt than in nickel, despite the tendency of the latter ones to lose their outermost part

of external oxide by shear rupture. The external TiO_2 layer tended to be thicker for the nickel–richest alloys: this suggests an easier outwards diffusion of titanium, which can be explained by the easy availability of the Ti atoms only present in solid solution in the matrix. If it is clear that Ti really diffused outwards for all alloys (demonstrated by the gradient existing in all the Ti concentrations profiles), oxygen also entered the alloys and diffused inwards. Oxygen met easier Ti (and Cr) to form internal TiO_2 and $TiCr_2O_4$ in their subsurfaces in the case of the nickel – richest alloys than in the cobalt – richest alloys, since Ti was more available in solid solution in the former alloys than in the later ones. This resulted in more extended internal oxidation involving Ti for the nickel–richest alloys than for the cobalt–richest ones, as observed in cross–section.

Concerning again the outward Ti diffusion during oxidation of the nickel–richest alloys, this destabilized the not many TiC existing in the ones of these alloys which contained some cobalt, and the depth of disappearance of TiC was particularly important by comparison with the cobalt–richest alloys containing more TiC carbides and less Ti in solid solution consequently. However this ought to have no real impact on the mechanical properties of the alloys since these depths are low in all cases. What is much worrisome is the considerable change in morphology carbides resulting from the long exposure at elevated temperature for all the alloys: coarsening and almost spheroidization of the TiC as well as of the chromium carbides, with the loss of their Chinese script morphology for the formers and of their acicular shapes for the later. High temperature mechanical tests carried out on as–cast alloys and on their aged versions and the comparison of their results will teach us the consequences of these morphology changes of these hardening particles.

CONCLUSION

Titanium initially added to help forming MC carbides did not succeed in obtaining morphologically stable strengthening particles but it did not totally transform the high temperature oxidation behavior of the alloys which stay chromia–forming and a good oxidation resistance in the case of the nickel–richest alloys. The presence of titanium enhanced internal oxidation – which is without great importance – but also the presence of a thin but continuous outermost layer isolating chromia from oxidizing air. This particularity, which is the most noticeable contribution of titanium to the oxidation mechanism, may be a chance for the long term sustainability of the alloys in the field of deterioration by oxidation: by isolating chromia from the oxidant atmosphere, it can possibly limit the

re–oxidation of chromia in gaseous species – phenomenon particularly active at so high temperature – and then the chromium consumption. This possible beneficial effect will be verified by oxidation tests including thermogravimetric measurements to assess chromia volatilization rates and compare the ones for Ti–free alloys and for the same alloys added with titanium.

Acknowledgements

The authors wish to thank Mr. Lionel Aranda and Ghouti Medjahdi for their technical help.

References

1. C. T. Sims and W. C. Hagel (eds.): 'The Superalloys'; 1972, New York, John Wiley & Sons.
2. E. F. Bradley: 'Superalloys: A Technical Guide'; 1988, Metals Park, ASM International.
3. P. Kofstad: 'High temperature corrosion'; 1988, London, Elsevier applied science.
4. D. J. Young: 'High temperature oxidation and corrosion of metals'; 2008, Amsterdam, Elsevier.
5. M. J. Donachie and S. J. Donachie (eds): 'Superalloys – A technical guide (2nd ed.)'; 2002, Materials Park, ASM International.
6. J. Chen; Q. Huo; J. Chen; Y. Wu; Q. Li; C. Xiao; X. Hui; Tailoring the creep properties of second-generation Ni-based single crystal superalloys by composition optimization of Mo, W and Ti; Materials Science & Engineering A: Structural Materials: Properties, Microstructure and Processing, 799 (2021) n° article 140163.
7. L. Ouyang; R. Luo; Y. Gui; Y. Cao; L. Chen; Y. Cui; H. Bian; K. Aoyagi; K. Yamanaka; A. Chiba; Hot deformation characteristics and dynamic recrystallization mechanisms of a Co-Ni-based superalloy; Materials Science & Engineering A: Structural Materials: Properties, Microstructure and Processing, 788 (2020) n° article 139638.
8. P. Zhou; X. Gao; D. Song; Q. Liu; Y. Liu; J. Cheng; Role of Ru on the microstructure and property of novel Co-Ti-V Superalloy; Journal of Materials Research, 35(20) (2020) 2737-2745.
9. Y. Zhai; L. Yang; F. Xue; Y. Chen; S. Mao; Defects and their elemental distributions in a crept Co-Al-W-Ti-Ta single crystal superalloy; Crystals, 10(10) (2020) n° article 908.
10. Y. L. Ge; J. Y. Wang; Transformation of MC carbide in cast nickel-base superalloys; Praktische Metallographie, 20(11) (1983) 554-61.
11. X. Z. Qin; J. T. Guo; C. Yuan; J. S. Hou; H. Q. Ye; Thermal stability of primary carbides and carbonitrides in two cast Ni-base superalloys; Materials Letters, 62(15) (2008) 2275-2278.
12. A. Baldan; J. M. Benson; Electron microprobe investigation of carbides in an as-cast nickel-based superalloy single crystal; Zeitschrift für Metallkunde, 81(6) (1990) 446-451.
13. Z. Yu; L. Liu; X. Zhao; W. Zhang; J. Zhang; H. Fu; Effect of solidification rate on MC-type carbide morphology in single crystal Ni-base superalloy AM3; Transactions of Nonferrous Metals Society of China, 20(10) (2010) 1835-1840.
14. S. Skolianos; T. Z. Kattamis; M. Chen; B. V. Chambers; Cast microstructure and tribological properties of particulate TiC-reinforced Ni-base or stainless steel matrix composites; Materials Science & Engineering A: Structural Materials: Properties, Microstructure and Processing, 183(1-2) (1994) 195-204.
15. B. Zheng; T. Topping; J. E. Smugeresky; Y. Zhou; A. Biswas; D. Baker; E. J. Lavernia; The influence of Ni-coated TiC on laser-deposited IN625 metal matrix composites; Metallurgical and Materials Transactions A: Physical Metallurgy and Materials Science, 41A(3) (2010) 568-573.
16. M. Khair; P. Berthod; As-Cast Microstructures and Hardness of Chromium-Rich Cobalt-Based Alloys Reinforced by Titanium Carbides; Materials Science: An Indian Journal, 14(13) (2016) 102-109.
17. M. Khair; P. Berthod; Thermodynamic and experimental study of cobalt-based alloys designed to contain TiC carbides; Calphad, 65 (2019) 34-41.
18. P. Berthod; S. Michon; L. Aranda; S. Mathieu; J.C. Gachon; Experimental and thermodynamic study of the microstructure evolution in cobalt-base superalloys at high temperature; Calphad, 27 (2003) 353-359.
19. P. Berthod ; Y. Hamini ; L. Aranda ; L. Héricher; Experimental and thermodynamic study of tantalum-containing iron-based alloys reinforced by carbides: Part I —Case of (Fe, Cr)-based ferritic steels; Calphad, 31 (2007) 351-360.

20. P. Berthod; E. Conrath; As-cast microstructures and behavior at high temperature of chromium-rich cobalt-based alloys containing hafnium carbides; Materials Chemistry and Physics, 143 (2014) 1139-1148.

21. P. Berthod; E. Conrath; Microstructure evolution in bulk and surface states of chromium rich nickel based cast alloys reinforced by hafnium carbides after exposure to high temperature air; Materials at High Temperatures, 31(3) (2014) 266-273.

22. P. Berthod; J. P. Gomis; G. Medjahdi; Oxidation behavior and structure stability at 1250 °C of chromium-rich TaC containing cast alloys based on nickel and cobalt; Metallurgical and Materials Transactions A, 51(8) (2020) 4168-4185.

23. E. Conrath; P. Berthod; Kinetics of high temperature oxidation and chromia volatilization for HfC-containing nickel-based alloys; Oxidation of Metals, 81 (2014) 393-405.

24. S. R. Shatynski; The thermochemistry of transition metal carbides; Oxidation of Metals, 13(2) (1979) 105-118.

25. P. Berthod; Looking for New polycrystalline MC-reinforced cobalt-based superalloys candidate to applications at 1200°C; Advances in Materials Science and Engineering, (2017), Article ID 4145369, https://doi.org/10.1155/2017/4145369

FIGURES CAPTIONS

FIGURE 1. Electronic micrographs illustrating the microstructures of the studied alloys in their as–cast state (SEM/BSE, ×500).

FIGURE 2. Photographs of the two main faces of the six samples after oxidation .

FIGURE 3. Example of XRD pattern: here the oxidized surface of the 1Co4NiTi alloy.

FIGURE 4. Example of XRD pattern: here the oxidized surface of the 4Co1NiTi alloy.

FIGURE 5. Electronic micrographs illustrating the surface states of the oxidized alloys (SEM/BSE, ×250).

FIGURE 6. Electronic micrographs illustrating the surface states of the oxidized alloys (SEM/BSE, ×1000).

FIGURE 7. Thicknesses of the two main oxides constituting the continuous external scale: Cr_2O_3 and TiO_2 (outermost oxide).

FIGURE 8. Depth of presence of internal Cr_2O_3 / $TiCr_2O_4$ and TiO_2 in the subsurface.

FIGURE 9. Depths of disppearance of chromium carbides and titanium carbides.

FIGURE 10. Chromium (top) and titanium (bottom) contents in the outermost part of the alloys.

FIGURE 11. Concentrations profiles in chromium from the oxide scale / alloy interface (SEM/EDS); A: 0Co5NiTi, B: 1Co4NiTi, C: 2Co3NiTi, D: 3Co2NiTi, E: 4Co1NiTi, F: 5Co0NiTi.

FIGURE 12. Concentrations profiles in titanium from the oxide scale / alloy interface (SEM/EDS); A: 0Co5NiTi, B: 1Co4NiTi, C: 2Co3NiTi, D: 3Co2NiTi, E: 4Co1NiTi, F: 5Co0NiTi.

FIGURE 13. Electronic micrographs illustrating the initial and final microstructures in the bulk of the three Ni–richest alloys (SEM/BSE, ×1000).

FIGURE 14. Electronic micrographs illustrating the initial and final microstructures in the bulk of the three Co–richest alloys (SEM/BSE, ×1000).

TABLES

TABLE 1. Designation and chemical compositions of the studied alloys.

wt.%	M (*: Co, **:Ni)	Cr	Ti	C
0Co5NiTi	0*	25	1.6	0.4
1Co4NiTi	15*	25	1.6	0.4
2Co3NiTi	29*	25	1.6	0.4
3Co2NiTi	29**	25	1.6	0.4
4Co1NiTi	15**	25	1.6	0.4
5Co0NiTi	0**	25	1.6	0.4

TABLE 2. Identification by XRD of the oxides spalled of during cooling and collected in the ceramic shuttles.

XRD peaks	Spinel oxide	chromia	Titanium oxide
0Co5NiTi	/	Cr_2O_3	TiO_2
1Co4NiTi	$NiCr_2O_4$	Cr_2O_3	TiO_2
2Co3NiTi	$(Co,Ni)Cr_2O_4$	Cr_2O_3	TiO_2
3Co2NiTi	$CoCr_2O_4$	Cr_2O_3	TiO_2
4Co1NiTi	$CoCr_2O_4$	Cr_2O_3	TiO_2
5Co0NiTi	$CoCr_2O_4$	Cr_2O_3	TiO_2

TABLE 3. Identification by EDS of the oxides remaining on surface and observed on cross–sections.

Spot EDS	Internal oxides	External oxides
0Co5NiTi	TiO_2, $TiCr_2O_4$, Cr_2O_3	Cr_2O_3, TiO_2
1Co4NiTi	TiO_2, $TiCr_2O_4$, Cr_2O_3	Cr_2O_3, TiO_2
2Co3NiTi	TiO_2, $TiCr_2O_4$, Cr_2O_3	Cr_2O_3, TiO_2
3Co2NiTi	TiO_2, $TiCr_2O_4$, Cr_2O_3	Cr_2O_3, TiO_2
4Co1NiTi	TiO_2, $TiCr_2O_4$, Cr_2O_3	Cr_2O_3, TiO_2
5Co0NiTi	TiO_2, $TiCr_2O_4$, Cr_2O_3	Cr_2O_3, TiO_2, $CoCr_2O_4$, CoO